eLife

Reviewed Preprint
v1 • May 14, 2026
Not revised

For correspondence:
shanzhao@ynu.edu.cn

* Contributed equally

Competing interests: No competing interests declared

Funding: See page 20

Reviewing editor: Hao Zhu, The University of Texas Southwestern Medical Center, United States

Platelets promote acute liver injury via extracellular vesicles-mediated Aldolase A

Ruoxue Yang*, Jinghua Liu*, Kai Fu, Ting Wan, Yahui Li, Can Shen, Ling Yang, Keqin Wang, Zhao Shan

Yunnan Key Laboratory of Cell Metabolism and Diseases, Center for Life Sciences, School of Life Sciences, Yunnan University Affiliated Hospital, Yunnan University, Kunming, China

eLife Assessment

In this **useful** manuscript, Yang et al attempt to show that platelet recruitment to the liver via macrophages contributes to APAP-induced liver injury, but there were many areas where the data supporting the conclusions were **incomplete**. For example, the idea that platelets only affected KC glycolysis, but not the metabolism of other cells, to mediate the phenotype after injury is not adequately supported by the evidence. It is recommended to perform additional experiments to strengthen the conclusions.

https://doi.org/10.7554/eLife.111041.1.sa3

Abstract

Platelets have emerged as active regulators of acute liver injury (ALI), yet the molecular mechanisms underlying their pathogenic functions remain poorly defined. Here, we demonstrate that platelets exacerbate liver injury by metabolically reprogramming Kupffer cells (KCs). We show that platelets are actively recruited to the injured liver and communicate with KCs through extracellular vesicles (EVs), which deliver the glycolytic enzyme aldolase A (ALDOA) into recipient cells. This EV-mediated transfer induces a robust glycolytic switch in KCs, licensing their pro-inflammatory activation and amplifying hepatic injury. Using platelet-specific Aldoa knockout mice, we establish that platelet-derived ALDOA is essential for KCs metabolic reprogramming and disease progression *in vivo*. Pharmacological inhibition of ALDOA with Aldometanib markedly attenuated liver injury. Circulating ALDOA levels were elevated in patients with ALI and correlated with disease severity. These findings uncover a platelet–macrophage metabolic axis that drives ALI and nominate ALDOA as a therapeutic target and biomarker.

Introduction

Acute liver injury (ALI) is a life-threatening clinical syndrome characterized by rapid hepatocyte death, sterile inflammation, and loss of hepatic function, yet its cellular drivers remain incompletely defined (1, 2). ALI arises from diverse etiologies, including infections, toxins, and autoimmune disorders, with acetaminophen (APAP) overdose representing one of the most common causes (1, 2). A consistent clinical feature of patients with severe ALI is thrombocytopenia, manifested as a marked reduction in circulating platelet counts (3, 4). In our previous study, we observed that these “lost” platelets accumulate within the liver, suggesting a previously unappreciated and potentially pathogenic role for platelets in ALI (5).

Platelets are anucleate blood components classically known for their role in hemostasis, but they are increasingly recognized as active modulators of inflammatory and immune responses (6–11). Nevertheless, technical challenges in platelet isolation, culture, and *in vivo* lineage tracing have limited mechanistic studies of platelet function in many diseases, including acute liver injury.

Although platelet involvement in liver pathology has been suggested (5, 12), the precise molecular mechanisms by which platelets exert their effects remain poorly understood. Defining these pathways is essential for the development of targeted platelet-based therapeutic strategies.

Kupffer cells (KCs), the liver-resident macrophages strategically positioned within the hepatic sinusoids, serve as central orchestrators of hepatic immune responses (13, 14). Following liver injury, KCs integrate damage-associated signals and rapidly adopt dynamic functional states that can either exacerbate hepatocellular damage or promote tissue repair (15, 16). How KC fate decisions are regulated within the injured hepatic microenvironment remains a key unresolved question. A defining feature of inflammatory macrophage activation is metabolic reprogramming, in which a shift toward aerobic glycolysis, reminiscent of the "Warburg effect," fuels biosynthetic and pro-inflammatory programs in classically activated macrophages (17, 18). Whether a similar metabolic rewiring occurs in KCs during ALI, and how such changes might be imposed by non-immune cells such as platelets, has not been systematically explored.

Building on our previous discovery that platelets infiltrate the liver and physically interact with KCs (5), we hypothesized that platelet–KC crosstalk exacerbates ALI by reshaping KC function. In this study, we sought to define the pathological consequences of platelet–KC interactions and to identify the critical molecular mediators involved. We demonstrate that platelets transfer the glycolytic enzyme aldolase A (ALDOA) to KCs via extracellular vesicles (EVs), thereby driving a glycolytic surge that amplifies liver injury. Using platelet-specific Aldoa knockout mice, we establish the essential in vivo role of platelet-derived ALDOA. Moreover, pharmacological inhibition of ALDOA confers significant protection from liver injury, and circulating ALDOA levels are elevated in patients with ALI, underscoring the clinical relevance of our findings. Together, these results identify a novel platelet–KC metabolic axis in ALI pathogenesis and nominate ALDOA as a promising diagnostic biomarker and therapeutic target.

Results

Recruited platelets enhance glycolytic program in Kupffer cells

To investigate the role of platelets in APAP-induced liver injury (AILI), we established an AILI mouse model using wild-type C57BL/6J mice. Mice treated with APAP for 12 hours exhibited a significant increase in serum alanine aminotransferase (ALT) levels and extensive hepatic necrosis compared to PBS-treated controls, confirming the successful induction of the AILI model (Figure S1A, B). Immunofluorescence staining revealed a substantial infiltration of platelets into the liver following APAP injury (Figure S1C). Additionally, co-immunofluorescence staining of KCs and platelets revealed colocalization between these cell types, suggesting their interaction within the liver during AILI (Figure S1D). These findings are consistent with our previous study (5) and demonstrated that platelets are recruited to the liver and interact with KCs during AILI.

We next sought to characterize the response of KCs to APAP injury and determine whether these changes are influenced by platelets interactions. First, we isolated KCs from mice treated with APAP for 0, 6, and 12 hours and performed RNA sequencing (RNA-seq). Kyoto Encyclopedia of Genes and Genomes (KEGG) pathway enrichment analysis showed a notable upregulation in glycolysis/gluconeogenesis pathways in KCs from mice treated with APAP for 12 hours compared to 0 hours, indicating a metabolic shift in KCs upon APAP treatment (Figure 1A). Further comparison of glycolysis and oxidative phosphorylation (Oxphos)-related enzymes expression in KCs treated with APAP for 0, 6, and 12 hours demonstrated a time-dependent upregulation in glycolysis-related gene expression but not in Oxphos-related gene expression (Figure 1B and Table S1). The upregulation of glycolysis-related genes (*Slc2a1*, *Pfkfb3*, *Pkm*) expression at 12 hours post-APAP treatment was further confirmed by qRT-PCR (Figure S1E). These gene expression data suggest a progressive increase in glycolytic activity in KCs in response to APAP. Hypoxia-inducible factor 1 alpha (HIF-1α) is a transcription factor that drives glycolysis and amplifies inflammatory responses under hypoxic conditions (19), while interleukin-1 beta (IL-1β) is a pro-inflammatory

cytokine typically upregulated in proinflammatory macrophages (19). The results revealed a significant increase in the expression of these genes in KCs in response to APAP (Figure S1E). This suggests that KCs undergo a glycolytic switch during early AILI.

To determine if the recruited platelets were responsible for this metabolic reprogramming, we depleted platelets using an anti-CD41 antibody (α-CD41) prior to APAP challenge (Figure S2A). Immunofluorescence confirmed effective platelet depletion in the liver (Figure S2B). Consistent with previous studies (5, 12), platelet depletion reduced liver injury, as indicated by a decrease in necrotic area and lower serum ALT levels (Figure S2C and D). To further explore the effects of platelet depletion on the KC glycolytic program, we isolated KCs from both platelet-depleted and control mice for RNA-seq analysis. Gene Set Variation Analysis (GSVA) of metabolic pathways in KCs from APAP-injured mice revealed that platelet depletion significantly downregulated the glycolysis pathway (p=0.038) (Figure 1C). Consistent with this, a heatmap showed that the expression of glycolysis-related genes induced by APAP was suppressed in KCs from platelet-depleted mice, while OXPHOS-related genes were restored (Figure 1D). qPCR analysis further validated that the mRNA expression of glycolysis- and inflammation-related genes in KCs was significantly reduced upon platelet depletion (Figure S2E). This highlights the critical role of platelets in driving glycolytic pathways in KCs. Collectively, these results demonstrate that platelet depletion prevents the metabolic switch in KCs during acute liver injury, underscoring the pivotal role of platelets in regulating the metabolic and inflammatory responses of KCs.

Finally, to establish a direct causal link, we isolated mouse platelets and co-cultured them with isolated KCs *in vitro*. We measured the extracellular acidification rate (ECAR) in KCs cultured with either conditional medium (Vehicle) or isolated mouse platelets (PLT). Consistent with the observations in KCs *in vivo*, KCs treated with platelets *in vitro* exhibited enhanced glycolytic activity (Figure 1E). Additionally, basal and maximal respiration rate was significantly increased in platelets-treated KCs, indicating elevated glycolytic activity (Figure 1F). This suggests that platelets augment glycolytic activity in KCs *in vitro*. Collectively, these findings demonstrate that platelets drive a metabolic reprogramming in KCs, characterized by enhanced glycolysis.

Kupffer cell glycolysis promotes APAP-induced liver injury

Having established that platelet-induced glycolysis in KCs is a key feature of the injury response, we next sought to determine whether this metabolic reprogramming functionally contributes to liver damage. To directly test this, we designed an experimental strategy to inhibit glycolysis specifically in KCs during APAP challenge using 2-deoxy-D-glucose (2-DG), a glycolytic inhibitor (20) (Figure 2A). To confirm the specificity of the effect to KCs, we included a group where KCs were depleted using clodronate liposomes (CLDN). We first validated the efficacy of our KC depletion protocol. Flow cytometric analysis of non-parenchymal liver cells confirmed that pretreatment with clodronate liposomes, but not control liposomes, effectively ablated the $CD11b^{low}$ $F4/80^{hi}$ Kupffer cell population (Figure S3). We then assessed the functional consequences of KC depletion and glycolytic inhibition. In KC-intact mice, administration of 2-DG alongside APAP challenge led to a significant reduction in both hepatic necrotic area and serum ALT levels compared to the PBS-treated APAP control (Figure 2B, C). Crucially, this protective effect of 2-DG was entirely absent in mice that had been depleted of KCs, demonstrating that the target of 2-DG's action is the Kupffer cell itself (Figure 2B, C). As expected, KC depletion alone was also protective against APAP injury. Finally, we analyzed the inflammatory state of the isolated KCs. qPCR analysis revealed that the mRNA expression of key inflammation-related genes, which were highly upregulated following APAP challenge, was significantly suppressed by 2-DG treatment (Figure 2D). This indicates that inhibiting the glycolytic program in KCs not only mitigates tissue damage but also directly quells their pro-inflammatory response. Together, these results demonstrate that the platelet-enhanced glycolytic program in Kupffer cells is not merely a correlative event but is a critical driver of the inflammatory response and subsequent liver injury following APAP overdose.

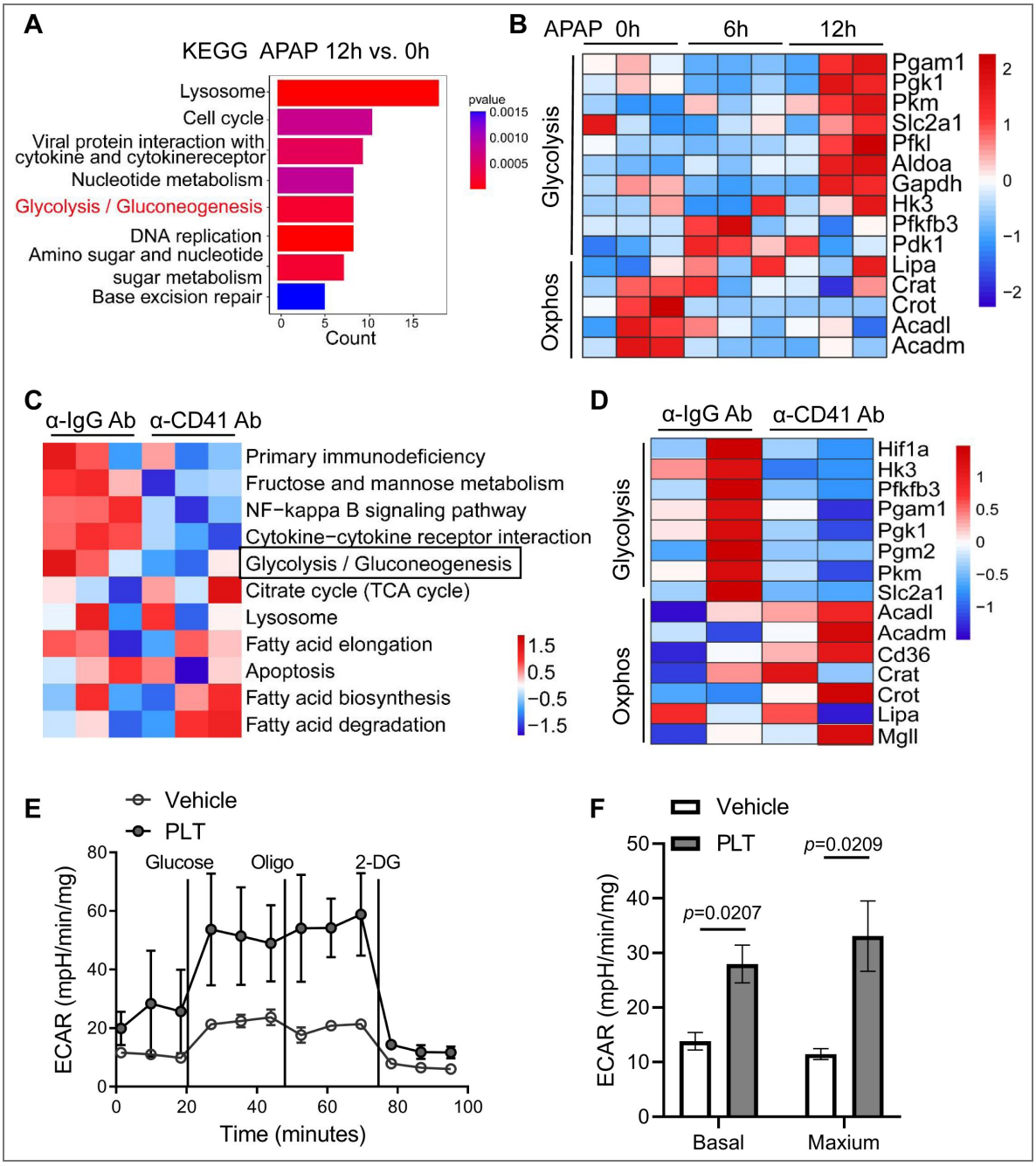

Figure 1. Recruited platelets enhance glycolytic program in Kupffer cells.

(A) KEGG pathway enrichment analysis of differentially upregulated genes in Kupffer cells (KCs) isolated from mice treated with APAP for 12 hours versus 0 hours (n=3 mice/group), based on RNA-seq. **(B)** Heatmap depicting the expression of glycolysis and oxidative phosphorylation (OXPHOS) genes in KCs following APAP treatment. (n=3). **(C)** Gene Set Variation Analysis (GSVA) of metabolic and immune pathways in KCs from mice treated with control IgG (α-IgG) or platelet-depleting (α-CD41) antibodies. The glycolysis pathway was significantly downregulated following platelet depletion (p=0.038). **(D)** Heatmap of glycolysis- and OXPHOS-related gene expression in KCs from mice treated with α-IgG or α-CD41 antibodies followed by APAP for 12 hours. **(E)** Extracellular acidification rate (ECAR) of KCs cultured alone or co-cultured with mouse platelets for 2 hours, measured in response to glucose, oligomycin, and 2-deoxy-D-glucose (2-DG) (n=3). **(F)** Basal and maximal respiration of KCs cultured alone or with platelets for 2 hours (n=3). p-value was calculated using an unpaired two-tailed Student' s t-test.

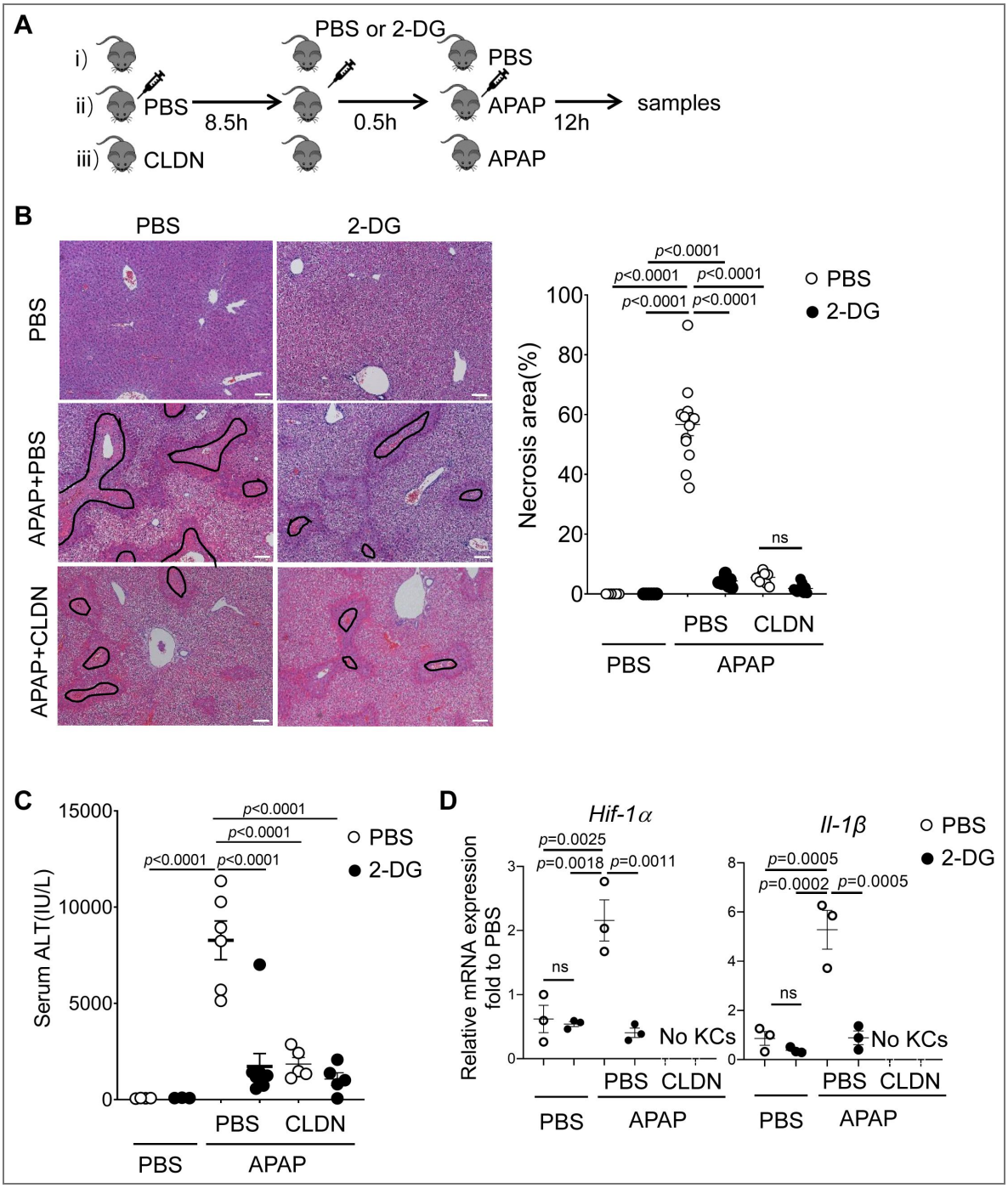

Figure 2. Kupffer cell glycolysis promotes APAP-induced liver injury.

(A) Experimental timeline to assess the role of Kupffer cell glycolysis in APAP-induced liver injury. Wild-type C57BL/6J mice were divided into three treatment regimens: i) Vehicle Control: Mice were treated with PBS or 2-deoxy-D-glucose (2-DG), followed 0.5 hours later by PBS for 12 hours. ii) KC-intact + APAP: Mice were pre-treated with control (PBS-loaded) liposomes for 8.5 hours, followed by PBS or 2-DG for 0.5 hours, and then challenged with APAP for 12 hours. iii) KC-depleted + APAP: Mice were pre-treated with clodronate liposomes (CLDN) to deplete Kupffer cells for 8.5 hours, followed by PBS or 2-DG for 0.5 hours, and then challenged with APAP for 12 hours. **(B)** Representative H&E-stained liver sections and quantification of necrotic area from mice in (A). Necrotic regions are outlined in black, and the percentage of necrotic area was quantified in each picture. Scale bars: 100 μm. **(C)** Serum alanine aminotransferase (ALT) levels from mice in (A). **(D)** mRNA expression levels of inflammation-related genes in Kupffer cells (KCs) isolated from mice in (A), measured by qPCR. Data in (B-D) were analyzed by one-way ANOVA followed by Tukey' s multiple-comparisons test.

Platelets-derived extracellular vesicles promote glycolysis in Kupffer cells

We next sought to identify the mechanism by which platelets communicate with Kupffer cells to drive glycolysis. We collected supernatant from isolated mouse platelets after a 2-hour culture and co-cultured KCs with either conditional medium (Vehicle) or platelet supernatant (PLT sup) for 2 hours. KCs exposed to platelet supernatant exhibited increased expression of glycolysis-related and inflammatory response-related genes compared to the vehicle controls (Figure 3A), suggesting that platelets secrete soluble factors capable of inducing a metabolic switch in KCs.

Previous studies have shown that platelets communicate with other cells through the release of EVs (21, 22). To investigate this further, we isolated platelet-derived extracellular vesicles (PEVs) and confirmed their identity by detecting established EV markers, including Tumor Susceptibility Gene 101 (TSG101) and Cluster of Differentiation 63 (CD63). High expression of both TSG101 and CD63 in the isolated PEVs confirmed their identity (Figure 3B). Transmission electron microscopy (TEM) analysis revealed that PEVs were a spherical vesicle with a bilayer membrane structure (Figure 3C), and the nanoparticle tracking analysis (NTA) detection results show that the particle size of PEVs were mainly distributed in the range of 59–288 nm, with the peak at 105 nm (Figure 3D).

To determine if these PEVs could directly modulate KC metabolism, we performed a Seahorse bioenergetic analysis. Kupffer cells co-cultured with isolated PEVs for just 2 hours exhibited a significantly elevated ECAR, indicating a robust increase in glycolytic flux (Figure 3E). Moreover, PEV treatment also enhanced the basal and maximal respiratory capacity of the KCs (Figure 3F), confirming PEV's effect on KC glycolysis.

Platelet-derived extracellular vesicles promote APAP-induced liver injury

Having established that PEVs can drive glycolysis in KCs *in vitro*, we investigated their role *in vivo*. We utilized a rescue approach in platelet-depleted mice (Figure 4A). Immunofluorescence confirmed the efficient depletion of platelets in the livers of all mice treated with the anti-CD41 antibody (Figure 4B). As expected, platelet-depleted mice were protected from AILI, showing minimal necrosis and low ALT levels. However, administration of isolated PEVs to these platelet-depleted mice restored the liver injury phenotype, as evidenced by significantly increased hepatic necrotic area and serum ALT levels (Figure 4C, D).

Finally, to confirm that PEVs directly target KCs *in vivo*, we intravenously injected PKH67-labeled PEVs and analyzed their localization. Immunofluorescence staining revealed that a significant number of F4/80-positive KCs had taken up the fluorescently-labeled PEVs within 3 hours of administration (Figure 4E). Collectively, these data identify PEVs as a critical communicator between platelets and KCs. PEVs are efficiently taken up by KCs, where they drive a potent glycolytic and inflammatory response that is essential to promote AILI.

ALDOA from PEVs induces a glycolytic switch in Kupffer cells

To identify the specific component within PEVs responsible for driving glycolysis in KCs, we isolated PEVs and performed a quantitative mass spectrometry analysis of their protein cargo, which identified 121 proteins (Figure 5A, Table S2). To refine this list and select for proteins specifically enriched in PEVs, we performed a comparative analysis with EVs derived from AML12 hepatocytes (Table S3). We excluded 53 proteins that were common to both PEVs and hepatocyte-derived EVs (HEVs), as well as cytoskeletal and coagulation-related proteins. This stringent filtering yielded a shortlist of seven candidate proteins: Aldolase A (ALDOA), Bridging integrator 2 (BIN2), Carboxylesterase 1C (CES1C), Inter-alpha-trypsin inhibitor heavy chain 2 (ITIH2), Murinoglobulin 1 (MUG1), Pleckstrin (PLEK), and Thrombospondin 1 (THBS1) (Figure 5A). Based on its central role as a catalytic enzyme in the glycolysis pathway, we selected ALDOA for further investigation. Western blot analysis confirmed the abundant presence of ALDOA within our preparations of

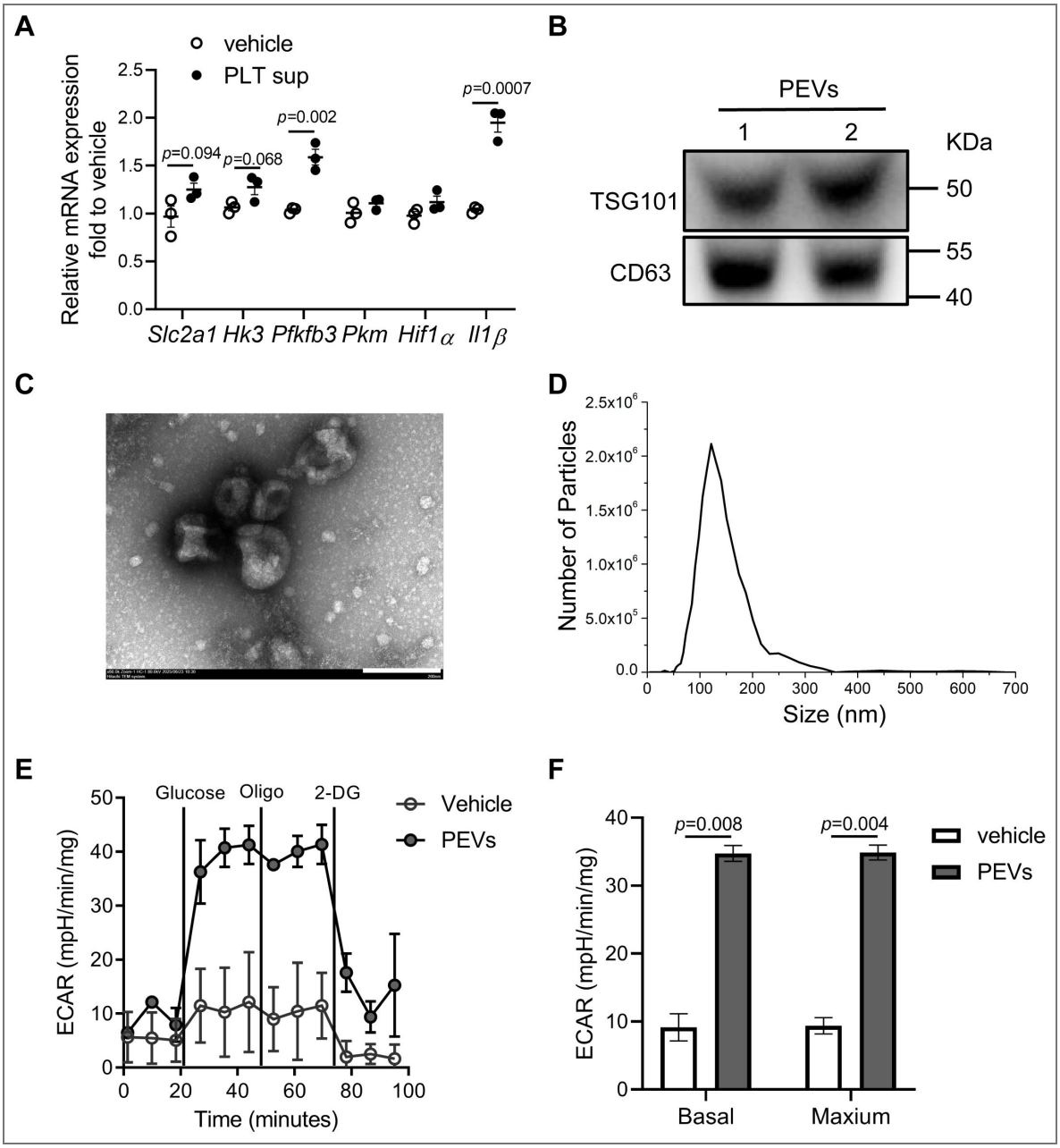

Figure 3. Platelets-derived extracellular vesicles promote glycolysis in Kupffer cells.

(A) mRNA expression levels of glycolysis and inflammation-related genes in Kupffer cells (KCs) treated for 2 hours with supernatant from in vitro-cultured platelets (PLT sup). **(B)** Western blot analysis confirming the expression of extracellular vesicle (EV) markers (TSG101, CD63) in platelet-derived extracellular vesicles (PEVs). **(C)** Representative transmission electron microscopy (TEM) image of isolated PEVs. Scale bar, 200 nm. **(D)** Representative nanoparticle tracking analysis (NTA) profile of the isolated PEVs. **(E)** Extracellular acidification rate (ECAR) in KCs cultured alone or with PEVs for 2 hours, followed by sequential injection of glucose, oligomycin, and 2-deoxy-D-glucose (2-DG). **(F)** Basal and maximal respiration rates in KCs cultured alone or with PEVs for 2 hours. Data in (A) and (F) were analyzed using an unpaired Student's t-test.

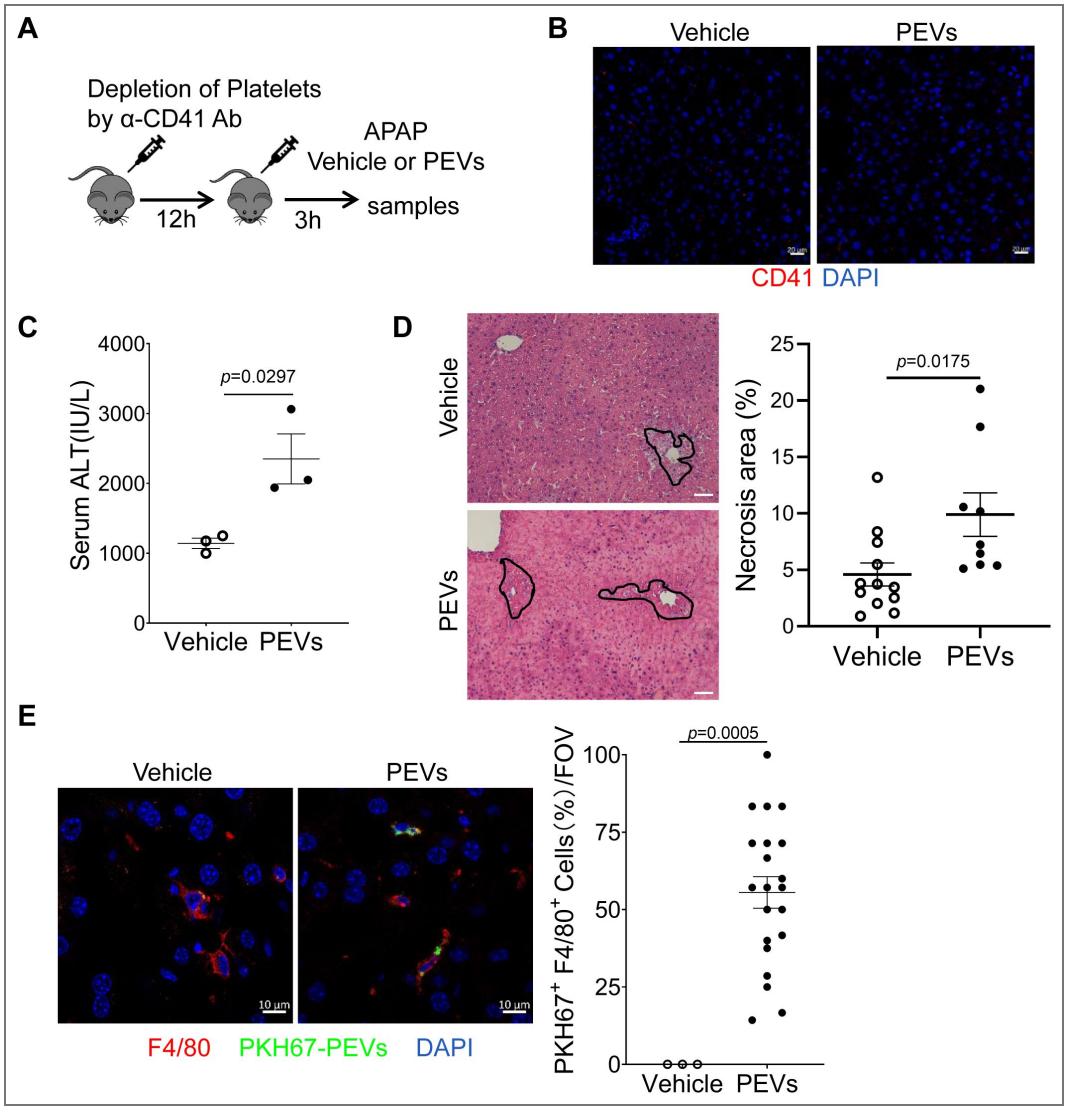

Figure 4. Platelet-derived extracellular vesicles promote APAP-induced liver injury.

(A) Experimental timeline to assess the role of PEVs in APAP-induced liver injury following platelet depletion. Wild-type C57BL/6J mice were depleted of platelets using an anti-CD41 antibody (α-CD41 Ab) and then treated with either Vehicle or PEVs concurrently with APAP for 3 hours (n=3 mice/group). **(B)** Immunofluorescence analysis confirming platelet depletion efficiency in liver sections from mice in (A), stained for CD41 (red) and counterstained with DAPI (blue) for nuclei. Scale bar, 50 μm. **(C)** Serum alanine aminotransferase (ALT) levels from mice in (A). **(D)** Representative H&E-stained liver sections and quantification of necrotic area from mice in (A). Necrotic regions are outlined in black, and the percentage of necrotic area was quantified in each picture. Scale bars: 100 μm. **(E)** Analysis of PEVs uptake by Kupffer cells *in vivo*. Mice were intravenously (*i.v.*) injected with PKH67-labeled PEVs for 3 hours. Liver sections were immunostained for Kupffer cells (F4/80, red) and nuclei (DAPI, blue). The number of PEVs-positive Kupffer cells was quantified. Data in (C-E) were analyzed by an unpaired two-tailed Student's t-test.

isolated PEVs (Figure 5B). To test its functional capacity, we treated KCs with recombinant ALDOA (rALDOA) protein. Seahorse metabolic analysis revealed that rALDOA potently enhanced the glycolytic capacity of KCs, as shown by a marked increase in the ECAR (Figure 5C), as well as basal and maximal respiration rate (Figure 5D).

To establish the *in vivo* relevance of ALDOA during AILI, we measured its serum levels over time in AILI mouse models. Western blot analysis revealed a dynamic increase in circulating ALDOA, which was detectable as early as 3 hours post-APAP treatment and remained elevated at 6 and 12 hours (Figure 5E). To determine if platelets were the source of this serum ALDOA, we depleted platelets in mice prior to APAP challenge. Platelet depletion significantly reduced serum ALDOA levels compared to the control IgG-treated group (Figure 5F), confirming that platelets are the primary contributors to the elevated ALDOA observed during injury. Together, these findings demonstrate that ALDOA is a specific and abundant protein cargo of PEVs. Upon delivery to KCs, ALDOA induces a profound glycolytic switch in KCs.

ALDOA serve as a potential therapeutic target for acute liver injury

To definitively establish the pathophysiological role of platelet-derived ALDOA, we generated platelet-specific Aldoa knockout mice (referred to as $PF4^{\Delta Aldoa}$ mice), with successful gene deletion confirmed by genotyping and western blot of platelet lysates (Figure S4A, B). Following APAP challenge, $PF4^{\Delta Aldoa}$mice exhibited a significant attenuation of liver injury, as demonstrated by markedly reduced serum ALT levels and a smaller hepatic necrotic area compared to their $Aldoa^{fl/fl}$ littermate controls (Figure 6A, B). To rule out the possibility that this protection was due to altered APAP bioactivation, we measured the levels of the metabolic enzyme CYP2E1 and the toxic metabolite NAPQI (23). We found no significant differences in hepatic CYP2E1 protein levels or NAPQI-protein adduct formation between the genotypes (Figure S5A), indicating that the protective effect was independent of the initial metabolic insult. Instead, KCs isolated from APAP-injured $PF4^{\Delta Aldoa}$ mice showed a significant downregulation of glycolysis- and inflammation-related genes (Figure S5B), confirming that platelet-derived ALDOA is critical for driving the pathogenic metabolic and inflammatory reprogramming of KCs *in vivo*.

We next investigated the therapeutic potential of pharmacologically inhibiting ALDOA after the initiation of injury. Administration of the ALDOA inhibitor Aldometanib (24) one hour after APAP overdose (Figure 6C) significantly protected against liver injury, as evidenced by lower serum ALT levels and reduced hepatic necrosis (Figure 6D, E). Again, this protection was not due to impaired APAP metabolism, as CYP2E1 and NAPQI-adduct levels were unaffected by Aldometanib treatment (Figure S6A). To assess the broader applicability of targeting this pathway, we tested its effect in a Concanavalin A (Con A)-induced immune-mediated liver injury model. Similar to APAP injury, KC depletion protected against Con A-induced hepatitis (Figure S7A, B). Importantly, administration of Aldometanib also significantly alleviated Con A-induced liver injury (Figure S7C-E), demonstrating that the ALDOA-driven pathogenic mechanism extends beyond AILI to immune-mediated hepatitis.

Finally, we sought to validate the clinical relevance of our findings in human disease. Re-analysis of a published proteomic dataset confirmed that ALDOA is a constituent of human platelet alpha-granules (25) (Figure 6F). Furthermore, analysis of EVs from patient serum revealed that EV-associated ALDOA levels were significantly higher in patients with polycythemia vera (26), a condition with hepatic involvement, compared to patients with Alzheimer's Disease (27) (Figure 6G). Most critically, in a cohort of patients with ALI, we found a strong and significant positive correlation between circulating ALDOA protein levels and serum ALT, a key clinical marker of hepatocyte damage (Figure 6H).

Collectively, these data demonstrate that genetic ablation or pharmacological inhibition of ALDOA is protective in multiple models of acute liver injury, operating through a mechanism that disrupt the secondary, inflammation-driven amplification of damage without affecting the initial insult. The presence and correlation of ALDOA with disease severity in human patients underscore its significant translational potential as a biomarker and a novel therapeutic target for acute liver injury.

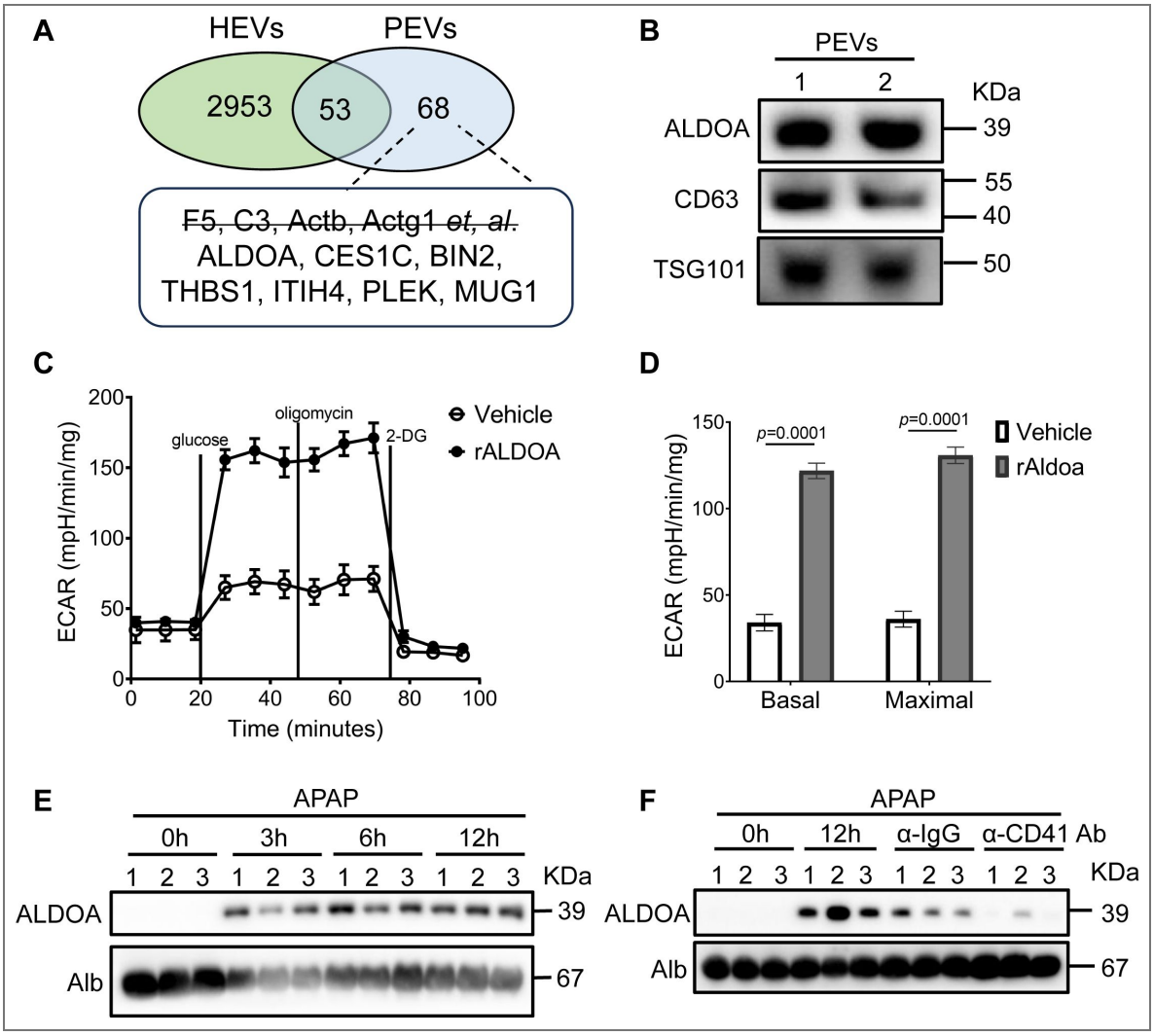

Figure 5. ALDOA from platelet-derived extracellular vesicles induces a glycolytic switch in Kupffer cells.

(A) Schematic workflow for identifying PEV-specific protein mediators. Proteins secreted by hepatocyte-derived EVs (HEVs) and those related to cytoskeleton and coagulation were excluded from the mass spectrometry analysis. Candidate proteins were defined as those appearing in all three independent replicates with more than two unique peptides. **(B)** Western blot analysis of ALDOA expression in isolated PEVs. CD63 and TSG101 were used as EV markers. **(C)** Extracellular acidification rate (ECAR) in Kupffer cells (KCs) treated with vehicle or recombinant ALDOA (rALDOA) for 2 hours, followed by sequential injection of glucose, oligomycin, and 2-deoxy-D-glucose (2-DG). **(D)** Basal and maximal respiration rates in KCs treated with vehicle or rALDOA for 2 hours. **(E)** Western blot analysis of ALDOA expression in mouse serum at different time points (0, 3, 6, 12 h) after APAP treatment (n=3). **(F)** Western blot analysis of ALDOA expression in serum from mice under various conditions: untreated (0 h), 12 h post-APAP, and 12 h post-APAP following platelet depletion with either a control IgG antibody (α-IgG Ab) or an anti-CD41 antibody (α-CD41 Ab) (n=3). Data in (D) were analyzed by an unpaired two-tailed Student's t-test.

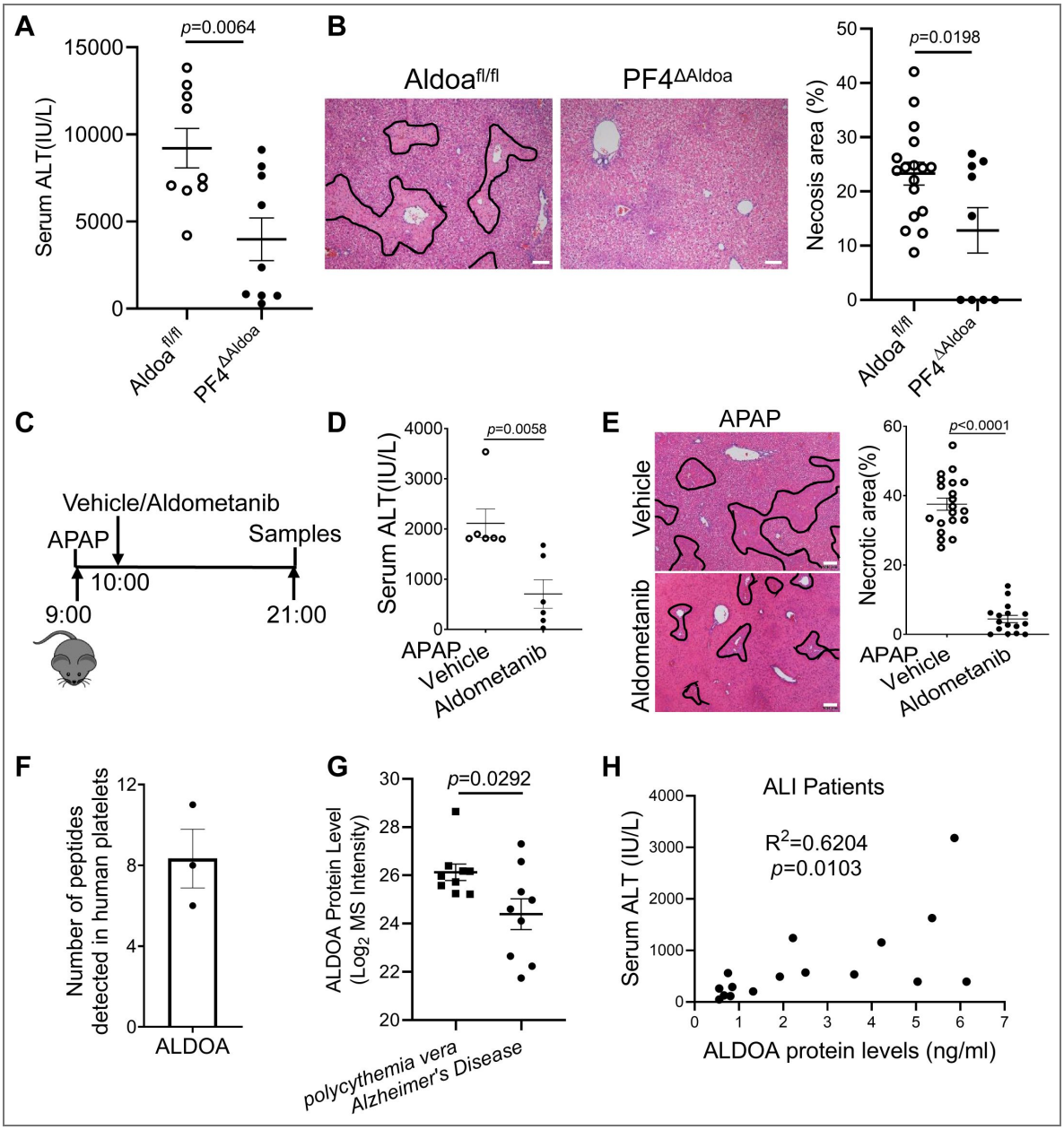

Figure 6. ALDOA serve as a potential therapeutic target for acute liver injury.

(A) Serum ALT levels were measured in *Aldoa*$^{fl/fl}$ and *PF4*$^{\Delta Aldoa}$ mice treated with 210mg/kg APAP for 24 hours. (n=9 mice/group) **(B)** Hematoxylin & Eosin (H&E) was performed to evaluate liver morphology in liver sections of mice in (A) (left). Necrotic areas were outlined in black, and the percentage of necrotic area was quantified (right) in each picture. **(C)** Experimental strategy for inhibiting ALDOA *in vivo* during AILI. Wild-type C57BL/6J mice were starved overnight (5 PM-9 AM), followed by an intraperitoneal injection of APAP at 9 AM. Mice were treated with 2 mg/kg Aldometanib one hour after APAP injection, and samples were collected 12 hours post-APAP. n=6 mice/group. **(D)** Serum ALT levels were measured in mice in (C). **(E)** H&E staining was performed to evaluate liver morphology in liver sections of mice in (C). Necrotic areas were outlined in black, and the percentage of necrotic area was quantified in each picture. **(F)** Platelets were isolated from healthy donors, and proteins were identified in the alpha granule fractions using liquid chromatography-tandem mass spectrometry (LC-MS/MS) as described by Maynard et al., 2007. **(G)** Extracellular vesicles (EVs) were isolated from serum of patients with polycythemia vera (*Fel et al*. (2019)) or Alzheimer's Disease (Nielsen et al. (2021)). Protein content within the EVs was characterized using liquid chromatography–tandem mass spectrometry (LC–MS/MS). Among the identified proteins, ALDOA intensity was quantified. **(H)** The correlation between ALDOA protein levels and serum ALT levels in patients with ALI (the detailed patients information is in Table S3). Correlations were evaluated by the Pearson correlation coefficient. (n=16) *p*-values were calculated using an unpaired two-tailed Student's t-test (A, B, D, E, G).

Discussion

The progression of AILI is a complex process involving not only the initial hepatocyte necrosis caused by NAPQI but also a robust sterile inflammatory response that amplifies the damage (28). While the role of immune cells like KCs has been acknowledged, the specific signals that activate them remain incompletely understood. In this study, we elucidate a novel and critical axis in which recruited platelets, via the release of EVs loaded with the glycolytic enzyme ALDOA, drive a pathogenic metabolic and inflammatory reprogramming of KCs, ultimately exacerbating liver injury. Furthermore, we identify ALDOA as a viable therapeutic target for ALI (Figure 7).

Our findings first confirm and extend previous observations that platelets are rapidly recruited to the liver following APAP overdose and physically interact with KCs (5). More importantly, we demonstrate that this interaction is not passive but functionally reprograms KCs metabolism. Through transcriptomic and functional analyses, we provide compelling evidence that KCs undergo a metabolic switch towards glycolysis during AILI, a shift that is entirely dependent on the presence of platelets. This platelet-induced glycolytic reprogramming is a key driver of pathology, as pharmacological inhibition of glycolysis within KCs significantly mitigated liver injury. This aligns with the established concept that a glycolytic switch in macrophages promotes a pro-inflammatory phenotype (29, 30), and our data place platelets as the upstream trigger for this switch in the context of sterile liver injury.

The central mechanistic discovery of our study is the identification of PEVs as the primary communicators in this cell-cell interaction. We show that PEVs are both necessary and sufficient to transmit the glycolytic signal to KCs. Adoptive transfer of isolated PEVs fully restored liver injury in platelet-depleted mice, providing direct evidence for their pathogenic role. This finding adds a new dimension to the understanding of platelet function in sterile inflammation, positioning them not only as coordinators of coagulation and inflammation but also as active regulators of cellular metabolism in recipient cells via vesicular communication (21, 22).

Our proteomic and functional investigations pinpointed ALDOA as the key protein cargo within PEVs responsible for inducing glycolysis in KCs. This is a particularly intriguing finding. While ALDOA is a canonical intracellular enzyme in glycolysis, its presence in the extracellular space and within EVs suggests a non-canonical, moonlighting function. We demonstrated that extracellular ALDOA alone can potently enhance glycolytic flux and the expression of inflammatory genes in KCs. The increase in circulating ALDOA during AILI, which originates predominantly from platelets, underscores its role as a damage-associated signal. Since PEVs can be phagocytosed by KCs *in vivo*, extracellular ALDOA is more likely internalized into KCs via EVs and influenced glycolysis pathway as a glycolytic enzyme.

The translational potential of targeting this pathway is strongly supported by our genetic and pharmacological studies. The protection observed in platelet-specific Aldoa knockout mice ($PF4^{\Delta Aldoa}$) confirms the *in vivo* relevance of our mechanistic model. Crucially, the protective effect of the ALDOA inhibitor Aldometanib, even when administered after APAP overdose, highlights a promising therapeutic window for intervention that targets the secondary inflammatory wave rather than the initial metabolic insult. This is a significant advantage, as it circumvents the narrow timeframe associated with N-acetylcysteine therapy (31). The efficacy of Aldometanib in both APAP and Con A-induced liver injury models suggests that the ALDOA-driven pathway is a common mechanism in diverse forms of ALI, potentially broadening its therapeutic applicability.

Finally, the clinical relevance of our findings is underscored by the analysis of human samples. The presence of ALDOA in human platelet granules and its elevated levels in serum EVs from patients with liver-involving diseases like polycythemia vera provide a crucial bridge from mouse models to human pathology. Most importantly, the strong positive correlation between circulating ALDOA levels and serum ALT in patients with acute liver injury positions ALDOA not only as a therapeutic target but also as a potential prognostic biomarker for disease severity.

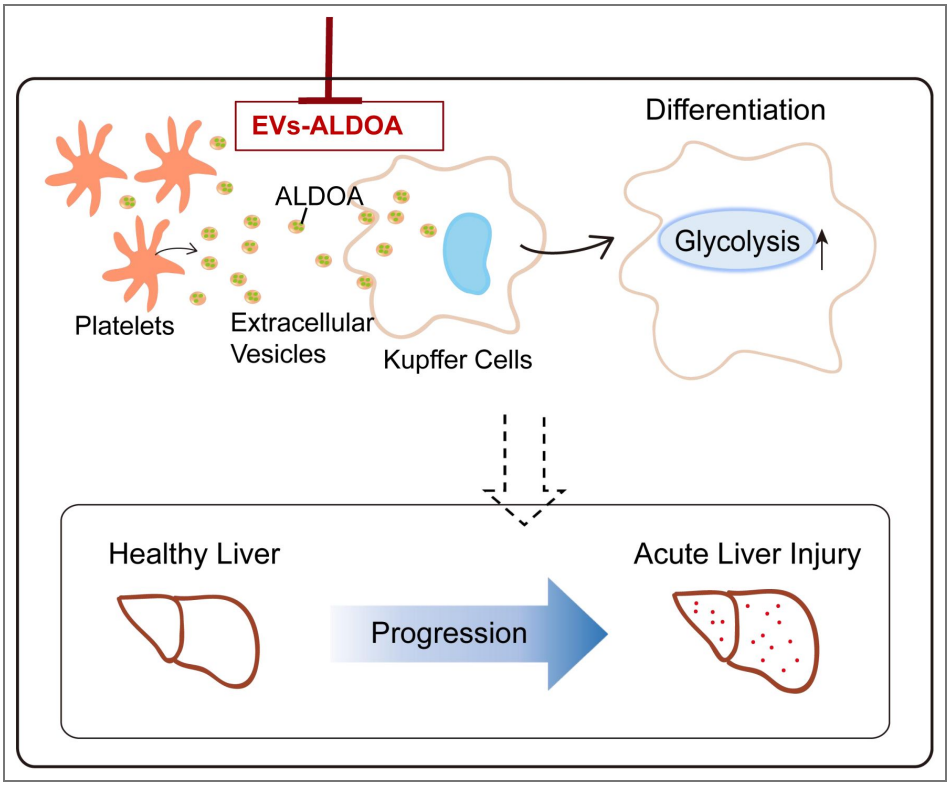

Figure 7. Platelets promote acute liver injury by transferring ALDOA to Kupffer cells via extracellular vesicles.

Platelet-derived extracellular vesicles (PEVs) deliver Aldolase A (ALDOA) to Kupffer cells, enhancing their glycolytic activity and driving acute liver injury. Targeting the ALDOA pathway in platelets represents a promising therapeutic strategy.

In conclusion, this study unveils a previously unrecognized pathway in the pathogenesis of ALI: Platelets → PEVs → ALDOA → KC Glycolytic Switch → Inflammatory Amplification → Hepatocyte Necrosis. By identifying ALDOA as a critical effector of this axis, our work opens up new avenues for therapeutic intervention. Targeting the ALDOA-mediated metabolic communication between platelets and KCs could represent a novel and effective strategy for treating ALI in patients.

Materials and Methods

Human sera

Serum samples from healthy volunteers and patients diagnosed with acute liver injury were collected at the Affiliated Hospital of Yunnan University (AHYNU), Kunming, China. The study was designed and carried out in accordance with the principles of AHYNU and approved by the Ethics Committee of AHYNU (Approval number 2024351). All patients provided written informed consent. Serum ALDOA levels in acute liver injury patients were quantified by western blot analysis, using 2 ng of recombinant ALDOA (rALDOA) as a standard, and band intensities were analyzed with ImageJ software.

Animal experiments and procedures

C57BL/6J mice (Strain No. N000013) were purchased from GemPharmatech. *Aldoa*$^{fl/fl}$ (Strain No. NM-KO-226330) were purchased from Southern Model Biotechnology Co., Ltd. To achieve platelet-specific deletion, *Aldoa*$^{fl/fl}$ mice were crossed with PF4-cre transgenic mice (Jackson Laboratory, Stock #008535), in which Cre recombinase expression is driven by the platelet factor 4 promoter. PF4-Cre; *Aldoa* $^{fl/fl}$ (*PF4*$^{\Delta Aldoa}$) mice and their Aldoa$^{fl/fl}$ littermates were used as controls. Genotyping was performed by PCR on genomic DNA extracted from tail clips using the following primers: *Aldoa* $^{fl/fl}$*:* F-GTTAGGCAAGCGCTCTGTTG, R-GTCAGCTTTATGGCCCCTGT. PF4-Cre: F1-CCAAG TCCTACTGTTTCTCACTC, R1-TGCACAGTCAGCAGGTT, F2-CTAGGCCACAGAATTGAAAGATCT, R2-GTAG GTGGAAATTCTAGCATCATCC. All the primers are from 5'end to 3' end.

All mouse colonies were maintained at the Laboratory Animal Center of Yunnan university. Animal studies described have been approved by the Yunnan University Institutional Animal Care and Use Committee (IACUC, Approval No. YNU20220262 for C57BL/6J strain, Approval No. YNU20240898 for *Aldoa*$^{fl/fl}$ strain, Approval No. YNU20220387 for PF4-Cre strain). For APAP treatment, mice (8-12 weeks old) were fasted overnight (5:00pm to 9:00am) before *i.p.* injected with APAP (Sigma, Cat #A7085) at a dose of 210 mg/kg for male mice. Male mice have been the choice in the vast majority of the studies of AILI reported in the literature (28, 32). Therefore, we used male mice in the majority of the experiments presented. However, we observed a similar phenotype in female mice as in male mice regarding the interaction between KCs and platelets(5). For Concanavalin A treatment, mice were *i.v.* injected with Saline or Concanavalin A (Sigma, Cat #C2010) at a dose of 15mg/kg. Liver paraffin sections and sera were harvested at time points indicated in the figure legends. H&E staining and ALT measurement (Teco Diagnostics, Cat #A524-150) were performed to examine liver injury.

Platelet depletion: WT mice were *i.v.* injected with anti-IgG (BD Pharmingen, Cat #553922, 2mg/kg) or anti-CD41 antibody (BD Pharmingen, Cat #553847, 2mg/kg) to deplete platelets at 12 hours before APAP treatment, followed by 210mg/kg APAP *i.p.* treatment for additional another 12 hours.

Kupffer cells depletion: WT mice were *i.v.* injected with 100 μL Clodronate liposomes (CLDN) to deplete Kupffer cells 9 hours before APAP or Con A treatment, followed by 210mg/kg APAP *i.p.* treatment or Con A treatment.

Inhibition of glycolysis: WT mice were *i.p.* injected with 250mg/kg 2-DG (Sigma, Cat# 8375, dissolved with PBS at a concentration of 50mg/mL) half an hour before APAP treatment, followed by 210mg/kg APAP *i.p.* treatment for additional another 12 hours.

Blocking endogenous ALDOA: WT mice were *i.p.* injected with 2mg/kg Aldometanib (MCE, Cat# HY-148189, dissolved with N-Methyl-2-pyrrolidone (Sangon Biotech, Cat# 872-50-4) at a stock concentration of 50mg/mL, diluted with PBS) one hour after APAP treatment, liver paraffin

sections and sera were harvested at 12 hours after APAP treatment.

PEVs labeling and injection: PEVs were isolated from mouse platelets culture supernatant by ultracentrifuge. And stained with PKH67 Green Fluorescent (sigma, Cat #MINI67) in 37°Cfor 30min. PEVs were washed with PBS for 1 time. And then collects PEVs by ultracentrifuge. WT mice were *i.v.* injected with anti-IgG (BD Pharmingen, Cat #553922, 2mg/kg) or anti-CD41 antibody (BD Pharmingen, Cat #553847, 2mg/kg) to deplete platelets at 12 hours before APAP treatment, followed by 210mg/kg APAP *i.p.* treatment and 20 μg PEVs (per mouse) *i.v.* treatment at the same time for additional another 3 hours.

Preparation of Kupffer cells

Wild-type C57BL/6J mice were anesthetized using a CO_2 chamber. To avoid contamination of the peritoneal cavity with fur, the skin and peritoneum were opened separately. The inferior vena cava was clamped with forceps, and a catheter was inserted into the superior vena cava via the right atrium. The portal vein was then cut once the buffer started to perfuse into the liver. The liver was perfused with 1× Hank's Balanced Salt Solution (HBSS) containing 53.6 mM KCl, 4.4 mM KH_2PO_4, 1367.5 mM NaCl, 3.36 mM $NaHPO_4$, 55.5 mM D-Glucose, and 100 mL 1 M HEPES (pH 7.2-7.4) for 3-5 minutes until it appeared clear. Subsequently, the buffer was switched to a collagenase digestion solution (1×HBSS with 1.25 mM $MgSO_4$, 4 mM $CaCl_2$, Collagenase Type I, and 50 μg/mL DNase) for 15-20 minutes of digestion. Post-digestion, the liver was dissected and placed in chilled 1×HBSS in a Petri dish to keep it cool until further processing. The gallbladder was removed, and the liver was chopped into 2-3 mm pieces and incubated in 10-20 mL digestion buffer at 37°C for 15 minutes. The liver tissue was then mashed using a 70 μm cell strainer placed over a 50 mL tube and rinsed with 1×HBSS to a final volume of 50 mL. The suspension was centrifuged at 50×g for 5 minutes (acceleration/brake = 0) to remove hepatocytes, with the resulting supernatant containing nonparenchymal cells (NPCs). The supernatant was further centrifuged at 450xg for 5 minutes (acceleration/brake ≥ 5), and the pellet, containing hepatic NPCs, was resuspended in 4 mL of 20% OptiPrep solution diluted with 1×HBSS. This suspension was carefully layered with 5 mL of 1×HBSS buffer in a 15 mL tube and centrifuged at 3000 rpm for 17 minutes (acceleration/brake = 0). The cell fraction between the 20% OptiPrep and 1xHBSS layers, containing KCs and liver endothelial sinusoidal cells (LESCs), was collected and washed with 1×HBSS.To isolate KCs, the cell fraction was incubated in a cell culture dish at 37°C for 10 minutes. KCs adhered to the plate, while LESCs remained in suspension. The adhered KCs were then collected for subsequent experiments. The purity and viability of isolated KCs reached 90% and 80%, respectively, which was confirmed by staining with anti-Timd4 antibodies or trypan blue.

Kupffer cells cultivated *in vitro*

KCs culture medium consisted of DMEM (VivaCell, Cat #C3113-0500) supplemented with 10% (vol/vol) fetal bovine serum (FBS, VivaCell, Cat #C04001-500), 100 IU penicillin, and 100 μg/mL streptomycin. KCs were cultured for 2 hours. For experiments involving KCs, $1 \times 10^{\wedge 6}$ cells seeded in one well of a 12-well plate were co-cultured with either $0.5 \times 10^{\wedge 6}$ isolated mouse platelets or vesicles isolated from $1 \times 10^{\wedge 6}$ isolated mouse platelets for 2 hours. After co-culture, the cells underwent various experiments including Seahorse assay, and RT-PCR. In another study, KCs were treated with platelet supernatant for 2 hours. Platelet supernatant was collected from isolated mouse platelets after a 2-hour culture. In additional experiments, KCs were treated with recombinant ALDOA for 12 hours. In some experiments, cells were treated with either vehicle or 5 μg/mL platelet-derived extracellular vesicles (PEVs) for 2 hours.

Isolation of mouse platelets

Blood was collected from CO_2-sacrificed mice via cardiac puncture using a 1/10 volume of ACD buffer (78 mM citric acid, 97 mM sodium citrate, 111 mM D-glucose, pH 7.4) as an anticoagulant. The collected blood was added to a 1.5 mL tube containing 300 μL of HT buffer (129 mM NaCl, 20 mM HEPES, 12 mM $NaHCO_3$, 2.9 mM KCl, 1 mM $MgCl_2$, 0.34 mM Na_2HPO_4, and 0.045 g of glucose per 50 mL of buffer, pH 7.3). Following centrifugation at 250×g for 3 minutes at 25°C, the

supernatant (platelet-rich plasma) along with the top one-third of the red cell layer was transferred to a new 1.5 mL tube. This mixture was centrifuged again at 250g for 3 minutes, and the supernatant was collected into another tube. An additional 200 µL of HT buffer was added to the previous tube, which was then centrifuged at 250×g for 3 minutes, and the resulting supernatant was pooled with the previous collection, resulting in approximately 600 µL of platelet-rich plasma. For functional studies, 50 ng/mL of PGI_2 (Sigma, Cat #P6188, 1 mg/mL in TBS, pH 7.3) was added to the platelet-rich plasma and incubated for 30 minutes at 37°C. The mixture was then centrifuged at 2000×g for 5 minutes to pellet the platelets. All centrifugation steps were performed with slow acceleration and deceleration settings.

Preparation of platelet-derived extracellular vehicles (PEVs)

Platelets were cultured in RPMI-1640 medium (VivaCell, Cat# C3001-0500) containing 10% exosome-depleted FBS, 100 IU penicillin, and 100 µg/mL streptomycin at 37°C for 2 hours. The culture medium was then collected and centrifuged at 500 g for 10 minutes at 4°C to remove cells. The supernatant was subsequently centrifuged at 2,000×g for 15 minutes at 4°C to remove cell debris. This process was followed by another centrifugation at 10,000×g for 15 minutes at 4°C to eliminate small cell debris. The remaining supernatant was used to isolate platelet-derived extracellular vesicles (PEVs) by ultracentrifugation at 30,000 rpm for 90 minutes at 4°C. The obtained PEV pellets were resuspended in an appropriate buffer. PEV-check antibodies TSG101 and CD63 were used to confirm marker expression profiles.

Transmission Electron Microscopy (TEM)

Isolated PEVs were resuspended in PBS. A 10 µL droplet of the PEV suspension was applied to a formvar-carbon coated copper grid for 1 minutes. The grid was then negatively stained with 2% uranyl acetate for 30 second, air-dried, and visualized using a Hitachi HT7800 transmission electron microscope operating at 120 kV.

Nanoparticle Tracking Analysis (NTA)

The size distribution and concentration of PEVs were analyzed using a ZetaView (Particle Metrix). PEVs were diluted in sterile PBS to achieve an optimal particle concentration for analysis. Three videos of 60 seconds each were captured for each sample, and the data were processed using ZetaView software (version 9.2).

In vitro cell culture

For experiments involving KCs, $1\times10\text{^}6$ cells seeded in one well of a 12-well plate were co-cultured with either $0.5\times10\text{^}6$ isolated mouse platelets or vesicles isolated from $1\times10\text{^}6$ isolated mouse platelets for 2 hours. After co-culture, the cells underwent various experiments including Seahorse assay, and RT-PCR. In another study, KCs were treated with platelet supernatant for 2 hours. Platelet supernatant was collected from isolated mouse platelets after a 2-hour culture. In additional experiments, KCs were treated with recombinant ALDOA for 12 hours. In some experiments, cells were treated with either vehicle or 5 µg/mL PEVs for 2 hours.

Sample preparation for flow cytometry analysis

Hepatic nonparenchymal cells (NPCs) were isolated as described previously(5). Briefly, mice were anesthetized and perfused according to the procedure for isolating Kupffer cells. After removing hepatocytes, the remaining cell suspension was centrifuged at 450 × g for 5 minutes to collect NPCs. The pellets were resuspended in 10 mL of 35% Percoll (Cytiva, Cat #17089109) and transferred to a new 15 mL tube. This was followed by centrifugation at 450 x g for 15 minutes to remove dead cells. Isolated liver NPCs were incubated with 1 µL of anti-mouse FcγRII/III (Invitrogen, Cat #14-0161-86) in FACS buffer (PBS + 0.2% FBS) to minimize non-specific antibody binding. The cells were then stained with anti-mouse CD45-APC 780 (Invitrogen, Cat #47-0451-82),

F4/80-PE (Invitrogen, Cat #12-4801-82), and CD11b-660 (Invitrogen, Cat #50-0112-82) for 30 minutes on ice. All antibodies were diluted 1:100. Flow cytometry was performed on an LSR Fortessa Cell Analyzer from BD Biosciences, and the data were analyzed using FlowJo software V10.

Histology and immunofluorescence staining

H&E Staining: Hematoxylin and eosin (H&E) staining was performed on paraffin-embedded liver sections. Briefly, liver tissues were harvested and fixed in 10% formalin for overnight, then dehydrated gradient alcohol. The tissues were subsequently embedded in paraffin and sectioned. H&E staining was performed using Hematoxylin (Biocare Medical, CATHE-M) and Edgar Degas Eosin (Biocare Medical, THE-MM). The necrosis areas were calculated using ImageJ.

Immunofluorescent Staining: Immunofluorescent staining was conducted on frozen liver sections. Fresh liver tissues were harvested and immediately fixed in 2% paraformaldehyde for 1 hour, washed with PBS three times, dehydrated in 30% sucrose at 4°C overnight, and finally embedded in OCT. Frozen sections (5 μm) were prepared and fixed with precooled acetone for 15 minutes at -20°C. The sections were permeabilized with 0.2% Triton X-100 in PBS and blocked with a blocking buffer (5% goat serum + 0.3% BSA in PBS). Following this, the sections were incubated with the primary antibody Purified Rat Anti-Mouse CD41 (BioLegend, Cat #553847, 1:200) overnight at 4°C in a humidified chamber. After washing with TBST, the sections were incubated with Alexa Fluor 488-conjugated Affinipure Goat anti-Rat secondary antibody (Jackson ImmunoResearch, Cat #112-545-003, 1:800) or Alexa Fluor™ 568 goat anti-Rat lgG(H+L) antibody (Invitrogen, Cat #A11077, 1:1000) for 1 hour at room temperature. For Kupffer cells co-staining, sections were further incubated with Alexa Fluor 594 anti-mouse F4/80 (BioLegend, Cat #123140, 1:200) or Alexa Fluor 647 anti-mouse CLEC4F (BioLegend, Cat #156804, 1:200) for 1 hour at room temperature. Finally, the sections were stained with DAPI (Beyotime, Cat #C1006) before mounting and imaging on an LSM 900 microscope (Zeiss). All images were collected using consistent parameters.

Sample Preparation for RNA Sequencing and Mass Spectrometry

Mice were treated according to different experimental protocols. KCs were isolated and lysed in 1 mL RNAiso Plus reagent (TaKaRa, Cat #9109). RNA concentration and purity were measured using a NanoDrop 2000 (Thermo Fisher Scientific), and RNA integrity was assessed using the RNA Nano 6000 Assay Kit on the Agilent Bioanalyzer 2100 system (Agilent Technologies). A total of 1 μg RNA per sample was used for RNA sample preparation. Sequencing libraries were generated using the NEB Next Ultra™ RNA Library Prep Kit for Illumina (NEB) following the manufacturer's recommendations. Index codes were added to attribute sequences to each sample. Clustering of the index-coded samples was performed on a cBot Cluster Generation System using the TruSeq PE Cluster Kit v4-cBot-HS (Illumina) according to the manufacturer's instructions. After cluster generation, the library preparations were sequenced on an Illumina NovaSeq 6000 platform, generating paired-end reads (the sequencing data for Fig1A-B were performed in BGI, and the sequencing data for Fig1C-D were performed in BMKCloud).

Mass Spectrometry Analysis of EV Cargo

To identify PEV-specific protein cargo, PEVs were isolated as described. For comparison, hepatocyte-derived extracellular vesicles (HEVs) were isolated from the culture supernatant of AML12, a mouse hepatocytes cell line, using an identical ultracentrifugation protocol. Protein extracts from PEVs and HEVs were trypsin-digested and analyzed by liquid chromatography-tandem mass spectrometry (LC-MS/MS) on a Orbitrap Exploris 480 MS (Thermo Fisher Scientific). Proteins identified in HEVs, as well as those annotated to the Gene Ontology (GO) ter ms "cytoskeleton" (GO:0005856) and "blood coagulation" (GO:0007596), were subtracted from the PEV proteome. Candidate proteins were defined as those present in all three biological replicates with more than two unique peptides.

RNA sequencing analysis

Raw data (raw reads) in fastq format were processed using in-house Perl scripts. Clean data (clean reads) were obtained by removing reads containing adapters, reads containing poly-N, and low-quality reads from the raw data. Quality metrics such as Q20, Q30, GC-content, and sequence duplication levels were calculated for the clean data. All downstream analyses were based on high-quality clean data. Reads were mapped against the reference genome and transcript annotation (GRCm38) using Hisat2 software. Further analysis was performed using RStudio (version 4.3). Differentially expressed genes were determined using the limma package, and enrichment analysis was conducted using clusterProfiler.

Western blot

Cells were lysed in RIPA lysis buffer (10mM Tris-HCl pH 8.0, 1mM SDTA, 0.5mM EGTA, 1% Triton X-100, 0.1%Ssodium deoxycholate, 0.1% SDS, 140mM NaCl, 100mM PMSF and 100 ×Cocktail were added freshly when using) on ice for 30 minutes. Protein extracts were obtained from the supernatants following centrifugation and subjected to SDS-PAGE. The membranes were blocked with 5% non-fat dry milk for 1 hour at room temperature. After blocking, membranes were incubated with primary antibodies followed by species-appropriate horseradish peroxidase-conjugated secondary antibodies. Membranes were washed three times with TBS-T and detected using either ECL Select Western Blotting Detection Reagent (Cytiva, Cat #RPN2235) or SuperSignal West Pico PLUS Chemiluminescent Substrate (Thermo Scientific, Cat #34580). For mouse serum, which will be diluted with PBS for 20 times, and then add SDS-loading buffer, 98℃ for 10min.

Primary antibodies used to detect specific proteins: ALDOA Polyclonal antibody (Proteintech, Cat #11217-1-AP, 1:5000), CD63 antibody (MX-49.129.5) (Santa Cruz, Cat #sc-5275, 1:500), TSG101 antibody(C-2) (Santa Cruz, Cat #sc-7964), Beta Actin Monoclonal antibody (Proteintech, Cat #66009-1-Ig, 1:10,000), Albumin Antibody (Cell Signaling Technology, Cat #4929, 1:1000), Alpha-Tubulin monoclonal antibody (Proteintech, 66031-1-Ig, 1:2000). Secondary antibodies include goat anti-Rabbit IgG (Jackson ImmunoResearch, Cat #111-035-003, 1:10,000), goat anti-Mouse IgG (Jackson ImmunoResearch, Cat #115-035-003, 1:10,000).

Seahorse Analysis

Real-time changes in extracellular acidification rate (ECAR) of KCs were measured using the XFe24 Seahorse extracellular flux analyzer (Agilent) with the Seahorse XF Glycolysis Stress Test Kit (Agilent, Cat #103020-100). KCs were plated onto XFe24 cell culture plates containing 0.3×10^6 cells a well and subjected to specific experimental treatments. The cells were rinsed with Seahorse XF basal medium supplemented with 2 mM glutamine and maintained in 500 µL of the same basal medium. The analysis was performed using the following Seahorse XF running buffers: Buffer A: 100 mM glucose in basal medium;Buffer B: 10 µM oligomycin in basal medium;Buffer C: 500 mM 2-deoxy-D-glucose (2-DG) in basal medium. At the end of the assay, the cells were lysed with RIPA buffer, and protein quantification was performed using the Pierce™ Protein Assay Kit (Thermo Scientific, Cat #23227) based on the bicinchoninic acid (BCA) method. Results were analyzed using Seahorse Wave Desktop Software (Agilent) and were normalized to protein content.

Prokaryotic purification of recombinant ALDOA

For the prokaryotic purification of recombinant Aldoa, the full-length cDNAs encoding Aldoa were cloned into the pET-28a vector and transformed into E. coli strain BL21 (DE3). The transformed cells were induced with 1 mM isopropyl-β-D-thiogalactopyranoside at an OD600 of 1.0 and incubated for an additional 4 hours at 37°C. Following incubation, the cells were collected and resuspended in ice-cold His binding buffer (20 mM Tris-HCl, pH 8.0, 500 mM NaCl, 1% Triton X-100, 1% glycerol, 5 mM imidazole). The cell suspension was sonicated and then centrifuged at 15,000 g for 1 hour at 4°C. The supernatant was filtered through a 40 µm filter membrane and subsequently purified using Ni-NTA Agarose. The Ni-NTA Agarose was washed sequentially with ice-cold His wash buffers: first with buffer 1 (20 mM Tris-HCl, pH 8.0, 500 mM NaCl, 1% glycerol, 20 mM

imidazole), followed by buffer 2 (20 mM Tris-HCl, pH 8.0, 500 mM NaCl, 1% glycerol, 40 mM imidazole). Recombinant Aldoa were eluted from the resin using ice-cold His elution buffer (20 mM Tris-HCl, pH 8.0, 500 mM NaCl, 1% glycerol, 500 mM imidazole) and its concentration was determined using a BCA assay.

Real-time RT-PCR assay

Total RNA was extracted from cells using RNAiso Plus reagent, followed by chloroform extraction and isopropanol precipitation to isolate RNA. The RNA pellets were washed with 75% ethanol, air-dried, and resuspended in DEPC-treated water. cDNA synthesis was carried out using the PrimeScript II 1st Strand cDNA Synthesis Kit (TaKaRa, Cat #6210A), adhering to the manufacturer's protocols. Quantitative RT-PCR (qPCR) was performed in duplicate using the PowerUp SYBR Green Master Mix (Applied Biosystems, Cat #A25742) on a StepOne system. The PCR conditions included an initial denaturation at 50°C for 2 minutes, followed by 95°C for 2 minutes, and then 40 cycles of 95°C for 15 seconds and 60°C for 1 minute. A final cycle involved 95°C for 15 seconds, 60°C for 1 minute, and 95°C for 15 seconds. Data were analyzed using the comparative Ct method with 18S rRNA as the internal control. Primer sequences are detailed in Table S4.

Analysis of Human Proteomics Data

For the analysis of human platelet alpha granules (Fig 6F), the raw mass spectrometry data from Maynard et al. were obtained and re-analyzed using Graphpad Prism software (v.8.0.2) to extract the spectral counts for ALDOA. For the analysis of EV proteomes from polycythemia vera and Alzheimer's disease patients (Fig 6G), processed data tables from Fel et al (PXD013234) and Nielsen et al (PXD024216) were directly obtained from the ProteomeXchange database as provided in the respective publications, and the normalized intensity values for ALDOA were extracted.

Statistical analysis

Statistical analyses were conducted using GraphPad Prism software (v.8.0.2). Data are expressed as mean values ± SEM. To assess significance between two groups, an unpaired two-tailed Student's t-test was employed. For comparisons among multiple groups, one-way ANOVA was used. Statistical significance was defined as $p < 0.05$. Detailed statistical information is provided in the figure legends and associated data. Images shown without biological replicates represent results from at least three independent experiments.

Data availability

RNA sequence data were deposited in GEO (accession number GSE274627). All data generated or analyzed during this study are included in the manuscript and supporting files; source data files have been provided for all figures.

Acknowledgements

We thank Dr. Bin Qi (Yunnan University) and Dr. Wenxiang Fu (Yunnan University) for suggestions and discussions. We thank Dr. Hao Yin (Wuhan University) for providing us with AML12 cells. This work was supported by National Natural Science Foundation of China (82570734 to Z.S.), Yunnan Provincial Science and Technology Department (C619300A086 to Z.S.), General Program of the Yunnan University Medical Research Fund (YDYXJJ2025-0040 to J. H. L.).

Additional information

Author Contributions

R. X.Y. conducted the experiments, analysed the data, and wrote the manuscript. J.H.L. provided the patient samples. T.W., Y.H.L., C.S., and L.Y. were responsible for patient sample collection. K.F. performed the transmission electron microscopy analysis of PEVs. K.Q.W. prepared the mass

spectrometry samples of HEVs. Z.S. conceived and designed the study, supervised the project, and contributed to the writing and revision of the manuscript.

Funding

Funder	Grant reference number	Author
MOST | National Natural Science Foundation of China (NSFC)	82570734	Zhao Shan
Yunnan Provincial Science and Technology Department (云南省科学技术厅)	C619300A086	Zhao Shan

Author ORCID iDs

Zhao Shan: https://orcid.org/0000-0001-5064-1023

Additional files

Supplementary figures.

Supplementary tables.

References

1. **Bernal W,** Auzinger G, Dhawan A, Wendon J (2010) Acute liver failure. *Lancet* **376**:190-201 https://doi.org/10.1016/s0140-6736(10)60274-7 | PubMed
2. **Lee WM** (2017) Acetaminophen (APAP) hepatotoxicity-Isn't it time for APAP to go away?. *J Hepatol* **67**:1324-1331 https://doi.org/10.1016/j.jhep.2017.07.005 | PubMed
3. **Tyagi T,** Jain K, Gu SX, Qiu MY, Gu VW, Melchinger H, Rinder H, et al. (2022) A guide to molecular and functional investigations of platelets to bridge basic and clinical sciences. *Nature Cardiovascular Research* **1**:223-237 https://doi.org/10.1038/s44161-022-00021-z | PubMed
4. **Hou Y,** Wang LJ, Wang HY, Sun L, Wang RT, Li YB, Hou M (2023) Platelet-Derived TGF-β1 Induces Functional Reprogramming of Myeloid-Derived Suppressor Cells in Immune Thrombocytopenia. *Blood* **142** https://doi.org/10.1182/blood-2023-182619
5. **Shan Z,** Li L, Atkins CL, Wang M, Wen Y, Jeong J, Moreno NF, et al. (2021) Chitinase 3-like-1 contributes to acetaminophen-induced liver injury by promoting hepatic platelet recruitment. *eLife* **10** https://doi.org/10.7554/elife.68571 | PubMed
6. **Wong CH,** Jenne CN, Petri B, Chrobok NL, Kubes P (2013) Nucleation of platelets with blood-borne pathogens on Kupffer cells precedes other innate immunity and contributes to bacterial clearance. *Nat Immunol* **14**:785-792 https://doi.org/10.1038/ni.2631 | PubMed
7. **Malehmir M,** Pfister D, Gallage S, Szydlowska M, Inverso D, Kotsiliti E, Leone V, et al. (2019) Platelet GPIbα is a mediator and potential interventional target for NASH and subsequent liver cancer. *Nature Medicine* **25**:641-655 https://doi.org/10.1038/s41591-019-0379-5 | PubMed
8. **Chauhan A,** Sheriff L, Hussain MT, Webb GJ, Patten DA, Shepherd EL, Shaw R, et al. (2020) The platelet receptor CLEC-2 blocks neutrophil mediated hepatic recovery in acetaminophen induced acute liver failure. *Nat Commun* **11**:1939 https://doi.org/10.1038/s41467-020-15584-3 | PubMed
9. **Groeneveld D,** Cline-Fedewa H, Baker KS, Williams KJ, Roth RA, Mittermeier K, Lisman T, et al. (2020) Von Willebrand factor delays liver repair after acetaminophen-induced acute liver injury in mice. *J Hepatol* **72**:146-155 https://doi.org/10.1016/j.jhep.2019.09.030 | PubMed
10. **Levoux J,** Prola A, Lafuste P, Gervais M, Chevallier N, Koumaiha Z, Kefi K, et al. (2021) Platelets facilitate the wound-healing capability of mesenchymal stem cells by mitochondrial transfer and metabolic reprogramming (vol 33, pg 283, 2021). *Cell Metabolism* **3**:688-690 https://doi.org/10.1016/j.cmet.2021.02.003

11. **Hoeft K,** Schaefer GJL, Kim H, Schumacher D, Bleckwehl T, Long QQ, Klinkhammer BM, et al. (2023) Platelet-instructed SPP1+macrophages drive myofibroblast activation in fibrosis in a CXCL4-dependent manner. *Cell Reports* **42** https://doi.org/10.1016/j.celrep.2023.112131 | PubMed

12. **Miyakawa K,** Joshi N, Sullivan BP, Albee R, Brandenberger C, Jaeschke H, McGill MR, et al. (2015) Platelets and protease-activated receptor-4 contribute to acetaminophen-induced liver injury in mice. *Blood* **126**:1835-1843 https://doi.org/10.1182/blood-2014-09-598656 | PubMed

13. **Guilliams M,** Bonnardel J, Haest B, Vanderborght B, Wagner C, Remmerie A, Bujko A, et al. (2022) Spatial proteogenomics reveals distinct and evolutionarily conserved hepatic macrophage niches. *Cell* **185**:379 https://doi.org/10.1016/j.cell.2021.12.018 | PubMed

14. **Ponti FFD,** Bujko A, Liu ZZ, Collins PJ, Schuermans S, Maueroder C, Amstelveen S, et al. (2025) Spatially restricted and ontogenically distinct hepatic macrophages are required for tissue repair. *Immunity* **58** https://doi.org/10.1016/j.immuni.2025.01.002 | PubMed

15. **Triantafyllou E,** Gudd CL, Mawhin MA, Husbyn HC, Trovato FM, Siggins MK, O'Connor T, et al. (2021) PD-1 blockade improves Kupffer cell bacterial clearance in acute liver injury. *J Clin Invest* **131** https://doi.org/10.1172/jci140196 | PubMed

16. **Deng ZH,** Loyher PL, Lazarov T, Li L, Shen ZY, Bhinder B, Yang HR, et al. (2024) The nuclear factor ID3 endows macrophages with a potent anti-tumour activity. *Nature* **626** https://doi.org/10.1038/s41586-023-06950-4 | PubMed

17. **O'Neill LAJ,** Pearce EJ (2016) Immunometabolism governs dendritic cell and macrophage function. *Journal of Experimental Medicine* **213**:15-23 https://doi.org/10.1084/jem.20151570 | PubMed

18. **Van den Bossche J,** O'Neill LA, Menon D (2017) Macrophage Immunometabolism: Where Are We (Going)?. *Trends in Immunology* **38**:395-406 https://doi.org/10.1016/j.it.2017.03.001 | PubMed

19. **Chen SZ,** Saeed AFUH, Liu Q, Jiang Q, Xu HZ, Xiao GG, Rao L, et al. (2023) Macrophages in immunoregulation and therapeutics. *Signal Transduction and Targeted Therapy* **8** https://doi.org/10.1038/s41392-023-01452-1 | PubMed

20. **Liu QX,** Li JX, Zhang WJ, Xiao C, Zhang SH, Nian C, Li JH, et al. (2021) Glycogen accumulation and phase separation drives liver tumor initiation. *Cell* **184**:5559 https://doi.org/10.1016/j.cell.2021.10.001 | PubMed

21. **Puhm F,** Boilard E, Machlus KR (2021) Platelet Extracellular Vesicles: Beyond the Blood. *Arteriosclerosis Thrombosis and Vascular Biology* **41**:87-96 https://doi.org/10.1161/atvbaha.120.314644 | PubMed

22. **Mabrouk M,** Guessous F, Naya A, Merhi Y, Zaid Y (2023) The Pathophysiological Role of Platelet-Derived Extracellular Vesicles. *Seminars in Thrombosis and Hemostasis* **49**:279-283 https://doi.org/10.1055/s-0042-1756705 | PubMed

23. **Hinson JA,** Reid AB, McCullough SS, James LP (2004) Acetaminophen-induced hepatotoxicity: role of metabolic activation, reactive oxygen/nitrogen species, and mitochondrial permeability transition. *Drug Metab Rev* **36**:805-822 https://doi.org/10.1081/dmr-200033494 | PubMed

24. **Zhang CS,** Li MQ, Wang Y, Li XY, Zong Y, Long ST, Zhang ML, et al. (2022) The aldolase inhibitor aldometanib mimics glucose starvation to activate lysosomal AMPK. *Nature Metabolism* **4**:1369 https://doi.org/10.1038/s42255-022-00640-7 | PubMed

25. **Maynard DM,** Heijnen HFG, Horne MK, White JG, Gahl WA (2007) Proteomic analysis of platelet α-granules using mass spectrometry. *Journal of Thrombosis and Haemostasis* **5**:1945-1955 https://doi.org/10.1111/j.1538-7836.2007.02690.x | PubMed

26. **Fel A,** Lewandowska AE, Petrides PE, Wiśniewski JR (2019) Comparison of Proteome Composition of Serum Enriched in Extracellular Vesicles Isolated from Polycythemia Vera Patients and Healthy Controls. *Proteomes* **7** https://doi.org/10.3390/proteomes7020020 | PubMed

27. **Nielsen JE,** Honoré B, Vestergård K, Maltesen RG, Christiansen G, Bøge AU, Kristensen SR, et al. (2021) Shotgun-based proteomics of extracellular vesicles in Alzheimer's disease reveals biomarkers involved in immunological and coagulation pathways. *Sci Rep* **11**:18518 https://doi.org/10.1038/s41598-021-97969-y | PubMed

28. **Ben-Moshe S,** Veg T, Manco R, Dan S, Papinutti D, Lifshitz A, Kolodziejczyk AA, et al. (2022) The spatiotemporal program of zonal liver regeneration following acute injury. *Cell Stem Cell* **29**:973-989. https://doi.org/10.1016/j.stem.2022.04.008 | PubMed

29. **Kelly B,** O'Neill LAJ (2015) Metabolic reprogramming in macrophages and dendritic cells in innate immunity. *Cell Research* **25**:771-784 https://doi.org/10.1038/cr.2015.68 | PubMed

30. **Freemerman AJ,** Johnson AR, Sacks GN, Milner JJ, Kirk EL, Troester MA, Macintyre AN, et al. (2014) Metabolic reprogramming of macrophages glucose transporter 1 (Glut1)-mediated glucose metabolism drives a proinflammatory phenotype. *Journal of Biological Chemistry* **289**:7884-7896 https://doi.org/10.1074/jbc.m113.522037 | PubMed

31. **Andrade RJ,** Aithal GP, Bjornsson ES, Kaplowitz N, Kullak-Ublick GA, Karlsen TH, Liver EAS (2019) EASL Clinical Practice Guidelines: Drug-induced liver injury. *Journal of Hepatology* **70**:1222-1261 https://doi.org/10.1016/j.jhep.2019.02.014 | PubMed

32. **Matchett KP,** Wilson-Kanamori JR, Portman JR, Kapourani CA, Fercoq F, May S, Zajdel E, et al. (2024) Multimodal decoding of human liver regeneration. *Nature* https://doi.org/10.1038/s41586-024-07376-2 | PubMed

Peer reviews

Reviewer #1 (Public review):

Summary:

In this manuscript, Yang et al expand on their previous work showing that platelet recruitment to the liver via liver macrophages is important for APAP-induced liver injury. Here, they show that platelets induce a glycolytic switch in liver non-parenchymal cells, including Kupffer cells, and that this is mediated by the protein Aldolase A produced by platelet-derived extracellular vesicles (PEV). They show that targeting Aldolase A may be a valid therapeutic strategy for severe APAP injury.

Strengths:

(1) They nicely showed that platelet effects in APAP are mediated by Aldoa via platelet-derived extracellular vesicles.

(2) Their data show that one of the effects of platelets in APAP liver injury is inducing metabolic switch to the glycolytic pathway, including in KCs.

(3) Their data points to the therapeutic potential of targeting ALDOA in severe APAP liver injury.

Weaknesses:

(1) They have not shown that the platelet-induced glycolytic switch is only in KCs.

(2) They also have not shown that KC's role in APAP injury is primarily mediated by their interaction with platelets and the subsequent glycolytic switch.

https://doi.org/10.7554/eLife.111041.1.sa2

Reviewer #2 (Public review):

Summary:

In this manuscript, the authors have investigated the role of platelet-derived ALDOA in liver injury induced acetaminophen (APAP) induced acute liver injury. There are some major flaws in data interpretation as described below. While a decrease in liver injury due to platelet

depletion and lower injury in platelet-specific ALDOA KO mice seems real, the claims related to EVs and Platelet-KC crosstalk are not well supported.

Strengths:

Core findings are interesting and supported by the data

Weaknesses:

(1) At least two additional timepoints, one at 6 hr and another at 24 hr should be performed in the APAP model to better understand the dynamics of liver injury, especially after platelet depletion.

(2) Interpretation of the experiments in Figure 2 with clodronate is flawed. 2-DG pretreatment and CLDN administration alone both seem to decrease liver injury substantially, so it is not surprising to see very little injury in the 2-DG+CLDN group.

(3) Since both 2-DG and CLDN were administered pre-APAP, it is possible that they may interfere with APAP metabolism. This should be checked by looking at GSH depletion at 30 min post APAP treatment. The same question goes for S2 figure data.

(4) There are no data on specific steps of APAP toxicity, such as GSH depletion, JNK activation, mitochondrial injury, etc., which are all well characterized in any of the studies. Rather, only injury endpoints are measured. It is critical to measure the mechanistic steps. This applies to all studies, but most importantly to the ALDOA-PF-KO mice in Figure 6.

(5) Interpretation of data in Figure 5F is flawed. Since depletion of platelets also decreases liver injury along with the platelets, it can not be deduced that the decrease in ALDOA is only in platelets. Many other things are changing.

https://doi.org/10.7554/eLife.111041.1.sa1

Reviewer #3 (Public review):

Summary:

The authors address the possibility that platelet (PLT) derived EVs are important mediators of acute liver injury. Furthermore, KCs are important mediators of inflammation and are noted to need to undergo metabolic reprogramming to achieve their effects during injury. They use an APAP-induced liver injury model (AILI). They show that PLTs are recruited and that they interact with KCs in this model system. RNA-seq of KCs showed upregulation of glycolysis and gluconeogenesis. PLT depletion led to reduced liver injury. RNA-seq of KCs showed downregulation of glycolysis. In vitro co-culture of KCs and pets recapitulated the glycolysis findings. In vivo, 2DG inhibited liver injury, but not in the setting of KC depletion. They went on to show that PLT-derived EVs mediate this effect on KCs using a mix of in vitro and in vivo assays, although control EVs were lacking. After doing mass spec on EVs, they find that ALDOA is the critical payload of the PEVs that mediates the pro-glycolytic effect in vivo. They both delete ALDOA from PLTs, and they use an ALDOA inhibitor to show that injury in AILI requires ALDOA.

Strengths:

This is generally an interesting series of observations with an elegant mechanism. Many of the experiments are done in vivo with highly rigorous KO models. However, in many of the EV experiments, there are concerns about a lack of appropriate controls that might limit the rigor of those aspects of the study.

Weaknesses:

(1) There is strong variability in the gene expression between mice in Figure 1B. I worry that the signals may not be statistically significant. The authors should assess the statistical significance.

(2) In Figure 2B, the necrosis areas that are circled in the image do not seem to resemble the quantitation on the right. For example, I don't see 60% necrosis in the APAP PBS group. Also, I don't see 5-10% necrosis in the CLDN APAP group. More images that are clearer are needed, and circled necrosis areas should be shown.

(3) In Figure 2D, a higher N should be shown. The number of mice (3) is different from the other experiments, so the exclusion of those mice should be explained.

(4) In general, control EVs from a non-PLT source should be used for all EV-related experiments. EVs derived from AML12 hepatocytes would seem to be a reasonable control for some of the experiments. Otherwise, it is hard to know if this is a general EV effect or one that is specific to PLT-derived EVs. In Figure 3B, EVs from non-PLTs should be used as a control. Since it is possible that all EVs express some level of TSG101 or CD63. In addition, control EVs should be used to test effects on KC metabolism, since the claim is that the effects are specific to PLT-derived EVs. Similarly, Figure 4 needs some kind of EV control that is not from PLTs.

(5) Figure 5B should include an EV control in the blot. Most of the blots need controls from AML12 EVs or from another in vivo source.

(6) It is a little difficult to imagine how enough ALDOA protein could be transmitted from PEVs to influence KC glycolysis on the gene expression level. It is possible that ALDOA is required for PLT-induced activation of KCs, or that EVs from PLTs can induce a metabolic shift in KCs. However, it has not been definitively shown that ALDOA from PEVs is directly causing the KC activation. Ultimately, it would be good to obtain PEVs from ALDOA WT and KO mice, then provide these PEVs to AILI mice without PLTs to see if they have differential effects on the AILI model. This would really demonstrate that the ALDOA in the PEVs is mediating the glycolytic, injurious effect.

https://doi.org/10.7554/eLife.111041.1.sa0